A Compound Eye-like Morphology Formed through Hexagonal Array of Hemispherical Microparticles Where an Alkyl-fullerene Derivative Self-assembled at Atmosphere-sealed Air/Water Interface

Ravindra Kumar Gupta[1], Hidehiko Asanuma[2], Juan J. Giner-Casares[2], Ayako Hashimoto[3], Tetsuya Ogawa[4] and Takashi Nakanishi[1,2,*]

[1] Research Center for Materials Nanoarchitectonics (MANA), National Institute for Materials Science (NIMS), 1-1 Namiki, Tsukuba 305-0044, Japan
[2] Department of Interfaces, Max-Planck-Institute of Colloids and Interfaces, Research Campus Golm, Potsdam 14424, Germany
[3] Center for Basic Research on Materials, National Institute for Materials Science (NIMS), 1-2-1 Sengen, Tsukuba 305-0047, Japan
[4] Institute for Chemical Research, Kyoto University, Kyoto 611-0011, Japan

*E-mail: NAKANISHI.Takashi@nims.go.jp

Received xxxxxx
Accepted for publication xxxxxx
Published xxxxxx

Abstract

Self-assembly processes are widely used in nature to form hierarchically organized structures, prompting us to investigate such processes at the macroscopic scale. We report an unprecedented approach toward the self-assembly of alkyl-fullerene (C_{60}) derivatives into a hexagonal array of hemispherical microparticles akin to the morphology of a compound eye. The method includes casting solvated alkyl-C_{60} compound on an air/water interface followed by controlled evaporation of the solvent under atmosphere-sealed conditions. This leads to the formation of a thin film floating on water with a diameter of up to 1.3 centimeters and exhibiting a hexagonally-packed hemispherical structure with a diameter of approximately 38 µm. Various measurements of the formed film reveal that amorphousness is necessary for suppressing uncontrollable crystallization, which affects the microparticle size and film formation mechanism. We tested the feasibility of this approach for the self-assembly of a relatively common C_{60} derivative, [6,6]-phenyl-C_{61}-butyric acid methyl ester ($PC_{61}BM$), resulting in the formation of a film with a similar pattern of hexagonally-packed larger microparticles approximately 152 µm in size of diameter.

Keywords: self-assembly, fullerene, interface, pattern, macroscopic film, compound eye

1. Introduction

Self-assembly processes are ubiquitous in nature [1]. Generally, soft structures in nature reversibly organize into

hierarchical architectures via various noncovalent interactions [2,3] and help to fabricate ordered aggregates from components with sizes from nanometers to micrometers [1]. The 'bottom-up' approach, i.e., the ability of molecules to selectively interact with neighboring molecules, plays a crucial role in generating highly organized molecular assemblies [1,4]. A rapid chemical precipitation method may sometimes facilitate synthesis and morphology control for various materials [5]. Two-dimensional (2D) nanoarchitectures have made substantial progress toward mimicking nature's scaffolds via covalent bonding [6-9], interfacial synthesis [10,11] including surfactant monolayer assisted interfacial synthesis [12-14], polymeric frameworks [15] and so forth [16-18]. Several techniques, such as on-surface polymerization [19], photopolymerization [20], and crystal engineering tactics [21], were also considered potentially useful methods for 2D polymer synthesis [22,23]. Nishihara et al. utilized liquid/liquid interfacial synthesis to create photo-functional nanosheets via three-way dipyrrin ligand and zinc acetate. A spontaneous reaction at the liquid/liquid interface developed a single-layered orange film with a 1-2 nm thickness, transferable to various substrates with a larger domain size of > 10 μm [10]. Dichtel et al. also demonstrated the interfacial polymerization of polyfunctional amines and aldehydes in a dioxane-mesitylene/water interface under the influence of a catalyst, generating a free-standing covalent organic framework film. The thickness of the uniform film was 2.5 nm, governed by its initial monomer concentrations [11]. Despite these significant efforts, the number of synthetic steps, tedious purifications, limitations on the accessible size and quantity of the products, and difficulties in their transfer from a surface to a substrate have impeded their practical application. The uniformity and monodispersity of organized 2D structures, incredibly hierarchical micrometer objects with long-range ordering, are often template-driven [24-29], such as honeycomb structure formation using condensed water droplets as template [17,26], 2D nanorod mesh formation on pre-existing benzoperylene microsheets [27] via crystal transformation, and so on. For instance, the formation of honeycomb architecture involves rapid evaporation of the solvent and induces the cooling of the solution surface, producing water condensation under high humidity. Surfactant dissolved water produces water droplets, which can prevent to fuse neighboring droplets and result in the hexagonal packing of the droplets in an energetically favorable on the molecular/polymeric film surface. Then, after evaporating water droplets, the resulting film forms a honeycomb structure [29]. Even metal-organic complexes self-assemble into randomly aggregated fibers with tunable emission [30]. Perhaps nucleation and growth mechanisms play a significant role in the self-assembly of small molecules, but achieving a homogeneous ordering in the entire film is always tricky. Instead of such difficult controllability of the perfect nucleation and growth processes, it could be achieved by an appropriate solvent selection, concentration, spreading of solvents, rate of solvent evaporation controlled by constant temperature, and intermolecular interactions between the organic molecules, even if there are no perfect crystalline ordering of small molecules. As described above, some achievements exist, especially regarding forming 2D molecular films with long-range ordering [31]. Achieving a 3D structure with a sub-centimeter pattern from the self-assembling of individual molecules remains an unprecedented challenge. Interfacial assembly of molecules and nanoparticles might lead to macroscopic films with ordering at the nanoscale, as shown in the seminal work by Dong and Murray in binary mixtures of inorganic nanoparticles [32]. However, such structuring relies on the patterning of pre-synthesized nanoparticles, and even then, no periodic structuring with a sub-millimeter pattern can be attained purely from self-assembly. This limitation arises mainly from the interactions between the nanoparticles and molecules during the assembly process, which is restricted to short range and leads to highly ordered nanostructures [33]. The pattern size will be limited to the template size (e.g., nanoparticles).

Here, we report a novel approach that can form a film with macroscopic ordering over a centimeter scale via a single procedure. A compound eye-like morphology was obtained by restricted evaporation of solvent from a drop-cast solution of an alkyl-fullerene (C_{60}) derivative at an atmosphere-sealed air/water interface without using any template. Here, we have systematically investigated and optimized the conditions required for obtaining the homogeneous architecture throughout the film. The kinetically controlled assembly is initiated via the formation of crystalline nano-aggregates and the growth of amorphous phase; in fact, the sequential growth represented by the amorphousness in the assembly is the critical factor to forming such well-defined hexagonally-packed hemispherical microparticles.

2. Experimental Section

2.1 Assembly at air/water interface

Unless otherwise noted, the experiments have been carried out at a controlled temperature (15 ± 1 °C, utilizing an incubator). All solvents used in this study were spectroscopic-grade reagents. Descriptions of fullerene derivative synthesis are available elsewhere [34]. Deionized water (>18 MΩ) was used throughout the experiment. A 50 mL vial was occupied by 36 mL of deionized water. The surface area of the water is 9.62 cm^2. 140 μL of **1** (3 mM in benzene, toluene, *m*-xylene, dichloromethane (CH_2Cl_2), or chloroform ($CHCl_3$)) was gently introduced onto the water

surface by micropipettes. After casting, the vial was capped and aged. The film formation depends on the evaporation rate of the solvent. With CH_2Cl_2 or CHCl3, **1** precipitate within a few hours. The film formation requires up to 48 hours for relatively slow evaporating solvents (benzene, toluene, or *m*-xylene).

2.2 Film transfer process

The film formed at the air/water interface was transferred by dipping a glass substrate attached to double-sided carbon tape on the surface, into the water and picking the film by sticking on the carbon tape.

2.3 Scanning electron microscopy

For scanning electron microscope (SEM) images, Philips XL30 electron microscope and JEOL NeoScope JCM-5000 were used at an accelerating voltage of 3 kV and 10 kV, respectively. All the microparticle arrays were lifted onto a silicon wafer (1 x 1 cm^2) or conductive carbon tape attached to the glass substrate from the water surface. After air-drying, samples were sputtered with gold prior to the measurement.

2.4 Small- and wide-angle X-ray scattering

The films obtained from various conditions were collected, dried (removal of adsorbed water), and powdered prior to filling in the glass capillary. The capillary was sealed by blowing from a fire gun and applied for Small- and wide-angle X-ray scattering (SWAXS) measurement. SWAXS measurements were performed using the Anton Paar SAXSess mc^2 instrument.

2.5 Focused ion beam and scanning ion microscopy

The aperture was milled on Mo foil using a focused ion beam (FIB) system (JEM-9310FIB, JEOL Ltd.). In both FIB and scanning ion microscopy (SIM) systems, the acceleration voltage was 20 kV.

2.6 High resolution-cryo-transmission electron microscopy

A sample dispersed in alcohol was deposited on a carbon-coated copper grid and then dried. A cryo-transmission electron microscopy (cryo-TEM) (JEM-2100F(G5), JEOL Ltd.) was used for high-resolution observation of the specimen to reduce sample damage by electron beam (cryo-protection). The acceleration voltage is 200 kV, and the sample stage is kept at 4.2 K by liquid helium.

2.7 Langmuir study

Experiments have been carried out in PTFE Langmuir troughs. A Wilhemy microbalance using a filter paper plate has monitored the surface pressure. An aliquot from 20 to 40 microliter of 1 mM solution of **1** has been cast onto the air-water interface. After a waiting time of 30 minutes for solvent evaporation, the layer was compressed with a barrier speed of 5 $cm^2\ min^{-1}$.

2.8 Langmuir-Blodgett deposition

The layer on the water surface was transferred onto a silicon wafer (for SEM measurements) or TEM grids, using the vertical dipping procedure (LB method) under constant pressure of ca. 30 mN m^{-1} and a lifting rate of 5 mm min^{-1}.

2.9 UV-Vis absorption and reflection spectroscopy

UV-Vis absorption of a homogeneous solution (**1** in *n*-hexane) [34] and solid state were measured on a JASCO V-670 spectrophotometer. For solid-state measurement, we have used $BaSO_4$ as the matrix. UV-visible reflection spectra at normal incidence as the difference in reflectivity (ΔR) of the dye film-covered water surface and the bare surface were obtained with a Nanofilm Surface Analysis Spectrometer (Ref-SPEC2 supplied by Accurion GmbH, Göttingen, Germany). Each reflection spectrum was acquired using an average of 10 spectra and an acquisition time of 20 milliseconds. Kinetic measurements were performed, recording a different reflection spectrum every 15 seconds for a total time of 10 minutes. Kinetic measurements on the formation of the monolayer were recorded for a total time of 10 minutes. The surface pressure was 0 mN m^{-1} for the whole experiment.

2.10 IR and IRRAS spectroscopy

Infrared spectroscopy of **1** in the solid state obtained under various solvent conditions was recorded on a Thermo Scientific Nicolet iS5 FT-IR spectrometer using the KBr method. Infrared Reflection Absorption Spectroscopy (IRRAS) detects molecular vibrations associated with changing molecular dipole moments. The signal is thus sensitive to the conformation and orientation of ordered alkyl lipid chains and to the structure of the headgroups. IRRAS spectra were collected by using an IFS 66/S FT-IR spectrometer (Bruker, Karlsruhe, Germany) equipped with a liquid-nitrogen-cooled MCT detector (narrow band mercury-cadmium-telluride detector) and a germanium coated KBr beam splitter. Spectra were recorded at a resolution of 8 cm^{-1} by using a Blackman–Harris four-term apodization. The IR beam from the spectrometer was focused onto the water surface of the Langmuir trough at an incidence angle of 428 (with respect to the surface normal). Parallel (p) polarization was used by using a KRS-5 polarizer. The experiments were performed in a trough containing two compartments connected by small channels. One compartment contained the buffer as a reference, and the second one contained the

sample with the monolayer. The reference signal was taken as background and was used to calculate the reflection–absorption spectrum of the monolayer under investigation to eliminate the water vapor signal. A constant water vapor level was achieved by placing the setup in a hermetically sealed box. The experiments were conducted at a constant temperature of 22 °C using a Lauda thermostat.

3. Results and discussion

3,4,5-Tri(eicosyloxy)phenyl *N*-methylfulleropyrrolidine (**1** [34,35], Figure 1) is intrinsically hydrophobic, and its self-assembly relies on van der Waals forces of alkyl chains and π-π interactions of C_{60} moiety [35-37]. Therefore, **1** act as a unique hydrophobic amphiphile. As a result of self-assembly in organic solvents, **1** produced various self-assembled solid superstructures of nanometer and micrometer size [36-38]. In particular, nanoflaked surface microparticles, which can be fabricated onto a substrate, exhibited a superhydrophobic property [36]. However, the uniformity of microparticle size was very poor. Therefore, the quality of a single layer of a microparticle array at the air/water interface was also low [36]. This low quality causes serious problems when we apply the fabricated surface for sensing and fine analytical purposes.

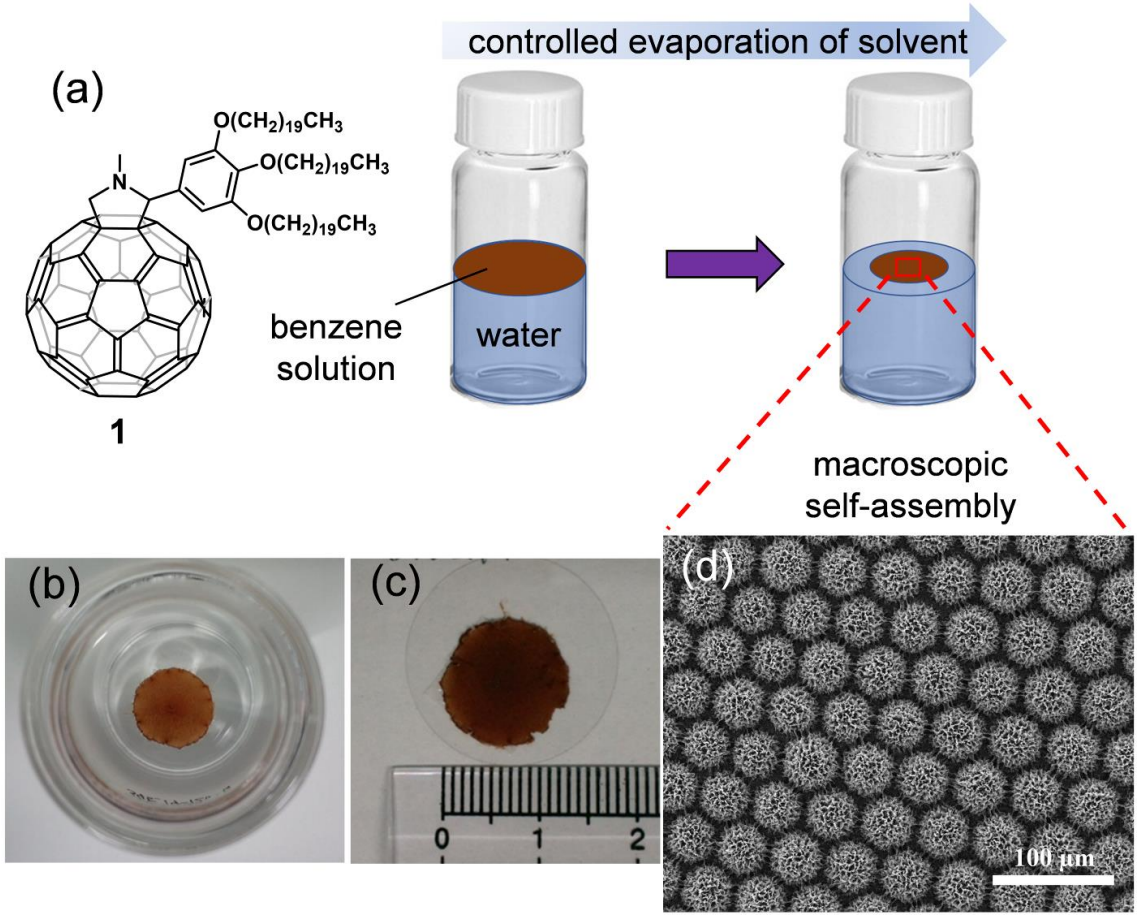

Figure 1. a) Solution of **1** (3 mM in benzene) cast on a water surface, upon restricted evaporation of solvent, precipitates a film at the atmosphere-sealed air/water interface at a controlled temperature of 15 °C; b) Precipitated floating film on water; c) transferred onto glass substrate, with measured diameter of approximately 1.3 cm; and d) an SEM image of the film exhibiting hexagonally-packed microparticle structure akin to compound-eye morphology.

The formation of a hexagonal array of hemispherical microparticles, akin to a compound eye-like structure exhibiting centimeter-scale ordering, is completely self-driven and requires a simple but careful procedure. One general approach is to cast solvated **1** onto the air/water interface, followed by reasonably slow solvent evaporation under atmosphere-sealed conditions over 48 h (Figure 1). However, diverging from the narrow preparatory condition will result in a different structure. Since they are formed under non-equilibrium conditions, i.e., air/water interface, and the molecules are situated only in the benzene phase, they are hemispherical (Figure 2). Although the local

monodispersity of the hemisphere is superior, as is evident from fast Fourier transform (FFT) analysis (Figure 2a), the dome size varies slightly depending on the radial area of the film. This is because the concave meniscus at the solute/water interface causes a surface concentration gradient of **1**. The micro-domes are composed of shaggy nanoflakes (Figure 1d) where the backside, which is in contact with the water surface, is relatively smooth, though the circular contour of the convex microparticles can be observed (Figure 2b). The cross-section of the microparticles, which was exposed by modification with a focused ion beam (FIB), proved that the microparticles are not hollow but are filled, as shown in the scanning ion microscope (SIM) image (Figure 2c).

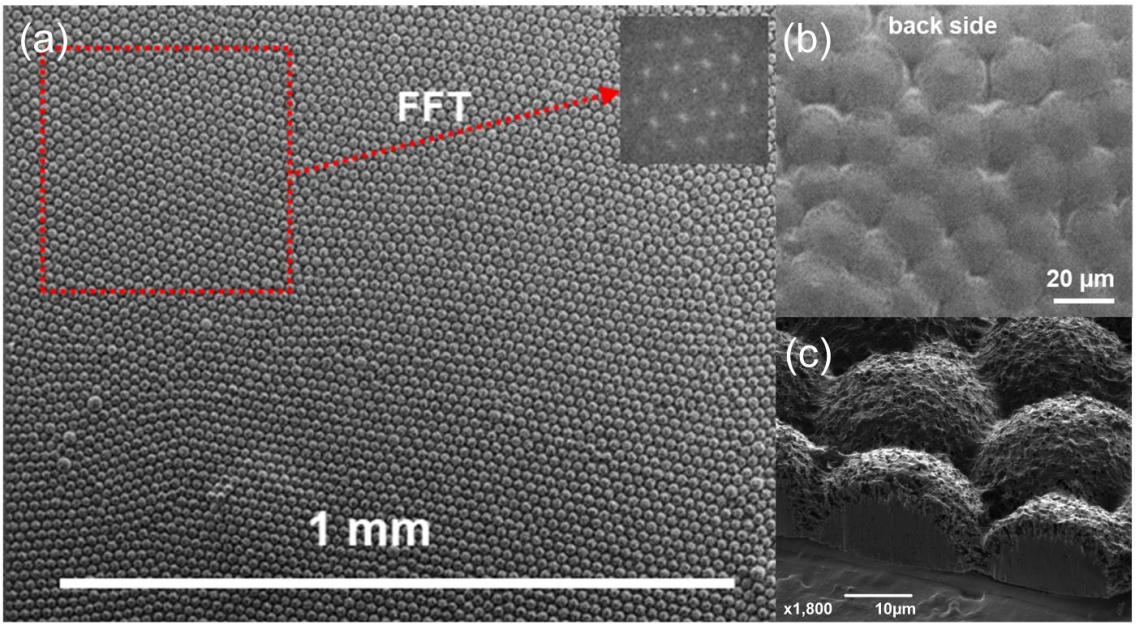

Figure 2. Self-organized hemispherical microparticle arrays of **1**. SEM images: a) top view in mm scale with FFT patterns; b) backside of the microparticle arrays; and c) SIM image of a cross-section of the microparticles prepared through FIB treatment.

To obtain a kinetically controlled macroscopic film on a centimeter scale (Figures 1b and 1c), we cast 140 μL of benzene solution of **1** (3 mM) over the water surface (surface area: 9.62 cm^2) and kept it at 15 °C for 48 h under atmosphere-sealed conditions, allowing slow evaporation of the solvent. The uniformity of the film solely depends on the type of solvent chosen. In addition to benzene, we investigated the film formation of **1** over the water surface with various solvents such as *m*-xylene, toluene, CH_2Cl_2, and $CHCl_3$. We kept all the conditions for film formation the same, but the resulting morphologies differed (Figure S1). A uniformly hexagonally-packed hemispherical array of centimeter length was best obtained from the benzene or toluene solution (Figures 1 and S1a). On the other hand, films were relatively featureless and appeared flatter from CH_2Cl_2 and $CHCl_3$ solutions (Figures S1c and S1d). More curved features were present with those assembled from toluene and *m*-xylene (Figure S1b), but the monodispersity of the microparticle diameter and quality of the film were not comparable with those via benzene. **1** dissolve well in all solvents employed here; therefore, the solubility difference is negligible with the concentration (3 mM). The other factor is the solvent evaporation rate. The films shown in Figure 1 only arise with relatively slow evaporation under atmosphere-sealed conditions (see methods for experimental details); an open environment without the lid of the glass bottle does not produce such well-ordered structures. Similarly, the evaporation rates of solvents differ and likely influence the film formation. Relative to *n*-butyl acetate (*n*-BuAc), CH_2Cl_2, $CHCl_3$, benzene, toluene, and *m*-xylene have evaporation rates of 27.5, 11.6, 5.1, 2.2, and 0.6, respectively. Although there is no quantitative measure to relate the concentration profile during solvent evaporation, it is known that the concentration gradient will be steeper upon quicker evaporation [39]. Upon fast evaporation, the local concentration **1** might be greater at the air/solute interface than at the solute/water interface. This kinetic parameter would play a delicate interface in the non-equilibrium process of solvent evaporation and **1** self-assembly. The different organizations obtained depend on the solvent evaporation, affecting self-assembly kinetics. It is known that different self-organized superstructures of alkyl-fullerene derivatives can be achieved by changing the conditions of assembly, like changing solvents leading to the formation of various assemblies with different morphologies, as shown in the literature [37]. For example, a fulleropyrrolidine with

3,4,5-(hexadecyloxy)phenyl showed various self-organized superstructures in various solvents; for instance, 2-propanol/toluene mixture generated vesicular aggregates, 1-propanol resulted in 1D fibrous structure and an equimolar mixture of water/THF yielded cone-shaped structure [37].

Applying solvents with different evaporation rates helps us conclude that only benzene and toluene are suitable matches for fabricating a film with a distinct hexagonal array of hemispherical morphology and macroscopic ordering. Therefore, to control the microparticle size (diameter) in the film, we carefully designed an experiment where **1** was dissolved in binary solvent (benzene/toluene system) with different volume ratios (75:25, 50:50, 25:75) and in neat benzene and toluene. The macroscopic film obtained under experimental conditions was subjected to SEM analysis. The film formed solely from benzene had a shorter microparticle–microparticle distance (37.6 ± 2.7 μm) in comparison to the film formed from toluene (52.2 ± 2.3 μm). Under binary solvent conditions, a benzene-toluene ratio of 75:25 does not significantly influence the microparticle–microparticle distance. When the ratio reaches 50:50, the distance increases drastically, and finally, the solvated **1** in toluene yields the longer microparticle–microparticle distance with larger diameter of microparticles (Figures S2 and S3). Thus, the microparticle–microparticle distance and microparticle size and the distribution of hemispherical domes in a macroscopic self-assembled structure can be controlled by varying the ratios of appropriate solvents used.

Surface tension is another parameter that controls the quality of film. Here, we optimized the surface tension of water, *i.e.*, 72.8 mN m^{-1} (Figure S4a), to form a uniform film. When the surface tension of water was lowered by adding methanol (5%, 10%, and 20%) [40], the microparticle diameter was less uniform. Still, the best flatness of the entire film was observed when using a 10% methanol-water system (Figure S4c). When the methanol content in water reached 20%, the surface tension decreased to 47.9 mN m^{-1}, generating random globular microparticles of smaller size (diameter; 8.4 ± 0.8 μm) and a rough surface film (Figure S4d). Even surface tension cannot finely control microparticle size, but in conclusion, water is optimum for forming a high-quality array of hexagonally-packed microparticles. The above two experiments (binary solvent ratios and surface tension) demonstrated that carefully choosing the balance of solvents and surface tension makes it possible to control the microparticle size and quality of the film.

SWAXS analysis was performed for the film of **1** prepared from benzene and *m*-xylene solution under atmosphere-open or atmosphere-sealed conditions (Figure 3a). Microparticles formed from 1,4-dioxane solution under heating-cooling reprecipitation showed strong reflection for the lamellar arrangement of **1**, with a *d*-spacing of 4.5 nm [36]. A film of **1** formed from benzene solution under air-open conditions at the air/water interface showed slightly broader reflections than the precipitated microparticles prepared from 1,4-dioxane solution, indicating less ordered arrangement of **1**. Regarding the film formed from the same solvent under atmosphere-sealed conditions at the air/water interface, it incorporated only broad reflections, showing somewhat amorphous nature of the film. Here, the broad reflections observed had larger angle positions than those observed under the air-open conditions, with diffraction at *q* of 1.57 nm^{-1}. In contrast, the film formed from *m*-xylene solution under atmosphere-sealed conditions showed rather dissolved and stronger reflections, which correspond to the typical A-B-A-B tilted lamellar arrangement as shown in the inset of Figure 3a (Figure S1b). The SWAXS pattern obtained from the benzene solution under an atmosphere-sealed condition is more similar to the film formed from the *m*-xylene solution, suggesting a tilted lamellar arrangement as the most probable basic ordered structure. The high-resolution cryogenic transmission electron microscopy (HR-cryo-TEM, Figure 3b) image of **1** prepared from the benzene solution under atmosphere-sealed conditions also supports a mostly amorphous region including a few bunches of nano-aggregates of **1** arranged in lamellar fashion. However, the well-arranged and ordered macroscopic structure in Figure 1 only arises when the film was prepared from benzene solution under atmosphere-controlled conditions at the air/water interface.

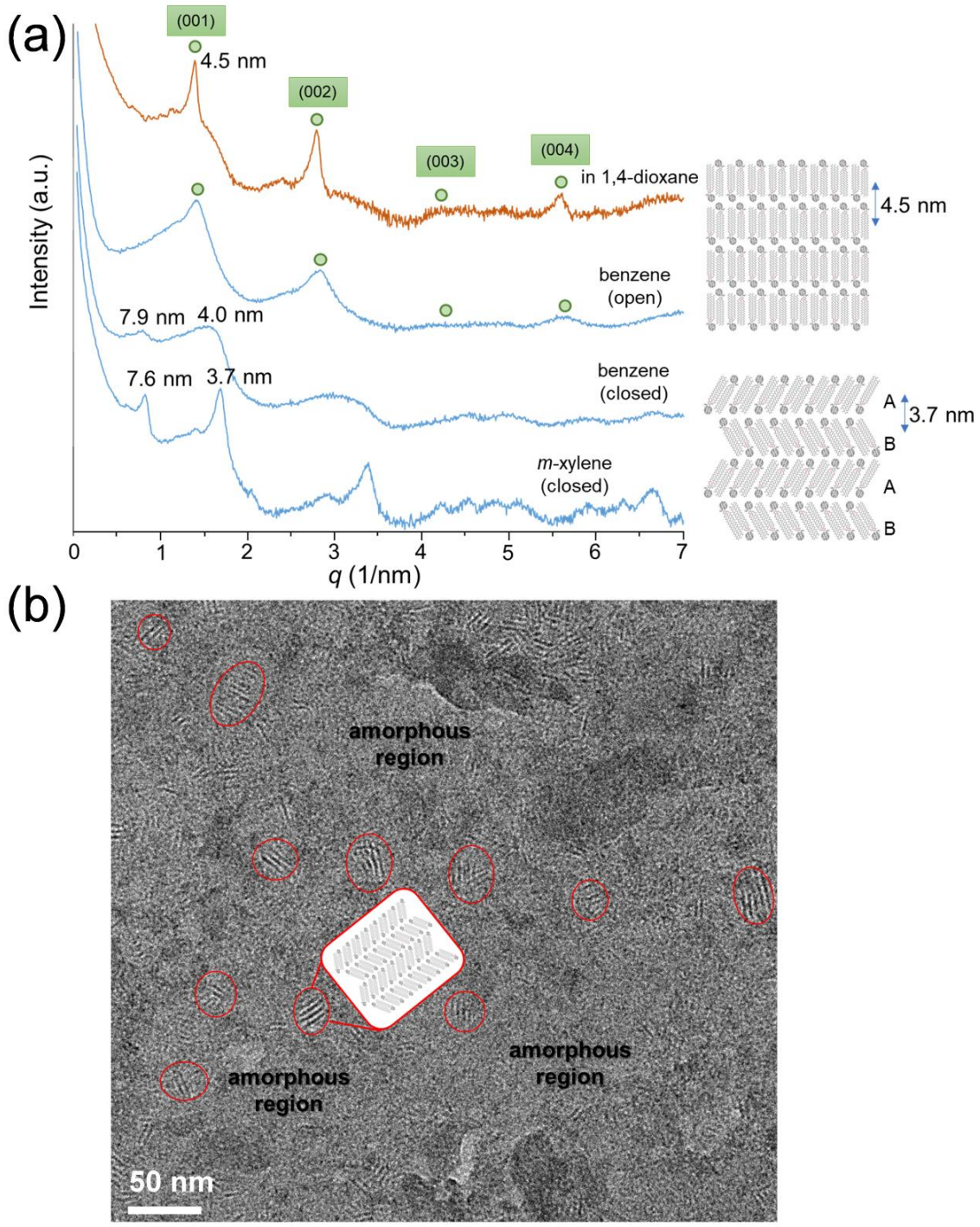

Figure 3. a) SWAXS patterns of film fabricated from various solvents under atmosphere-open and atmosphere-sealed conditions; b) HR-TEM image of **1** prepared from benzene solution under atmosphere-sealed condition, showing nano-aggregates composed of lamellar assemblies and mostly amorphous regions.

For further understanding of intermolecular interactions during the self-assembly process, films prepared from various solvents such as CH_2Cl_2, $CHCl_3$, benzene, toluene, and *m*-xylene were subjected to film state infrared spectroscopic measurement (Figure S5, Table S1). All films exhibited peaks at ~2850 and ~2918 cm^{-1}, assigned to the characteristic stretching vibrational modes of methylene unit, $\upsilon_{sym}(CH_2)$ and $\upsilon_{asym}(CH_2)$, respectively. At such frequencies, the alkyl chains are considered to be in crystalline-like states with all-trans conformation [41]. These wavenumbers are similar to those reported for other solid architectures of **1** [36]. Similarly, solid-state UV-Vis spectroscopy measurements under reflection mode were performed for the films of **1** mixed with $BaSO_4$ matrix, obtained from various

solutions at the air/water interface. The absorption maximum in all cases was in the range of 260–262 nm, but shoulder peaks varied from 217–228 nm and 325–332 nm, respectively (Figure S6, Table S2). This shows slight red-shifted absorption in the film state compared with that for the *n*-hexane solution of **1** [34], attributed to π-π electronic interactions among C_{60} moieties in the film state [36-38].

A concentration-dependent approach was performed to elucidate the growth mechanism of microparticles for film formation where 0.1, 0.5, 3.0, and 4.0 mM benzene solutions of **1** were prepared, and the films obtained from them were investigated. In the very dilute condition, *i.e.,* 0.1 mM solution, irregular growth of microparticles of 11.5 ± 2.6 μm in size was observed. An increase in concentration yielded a rise in microparticle size, *i.e.,* the 0.5 mM solution yielded 18.7 ± 2.4 μm center-to-center distance. A well-arranged macroscopic ordering was obtained under specific conditions (concentration: 3.0 mM), as shown in Figure 1, with a mean average flake size of 1.3 ± 0.1 μm. Increasing the concentration further (4.0 mM) did not lead to a fully grown hexagonal array of hemispherical particles (center-to-center distance: 14.5 ± 0.8 μm) but instead to the formation of ~45% thicker flakes (Figure S7). The 'thicker flakes' of hemispherical particles result in less flake-featured, relatively smoother surfaces of films. Fewer nuclei for the formation of hemispherical microparticles and a smaller number of molecules cannot support the full growth of microparticles in the condensed organic solution phase at the air/water interface. Retention time also plays a significant role in the growth of hemispherical microparticles at the solvent/air interface. **1** placed at the solvent/air interface, because of edge evaporation of the solvent, creates irregular growth, resulting in irregular microparticle size and short retention time for the growth of microparticles. Similarly, under high concentrations, interdigitation of flakes leads to hindered growth of microparticles with longer retention time, but thicker flakes are formed due to higher concentration. An ordered macroscopic assembly is generated only under optimized conditions (Figure 1).

To test the feasibility of our approach, we examined another relatively common C_{60} derivative, [6,6]-phenyl-C_{61}-butyric acid methyl ester ($PC_{61}BM$), using the same method and optimized by varying solvents as well as varying ratios of mixed solvents (Figure S8 and S9). As optimized conditions, 0.75 mM (60 μL) of a mixed solvent (benzene:cumene = 4:6 by volume ratio) solution of $PC_{61}BM$ was cast over the air/water interface (surface area of water surface: 4.9 cm^2) followed by very slow evaporation (for three weeks) of solvent at 15 °C under atmosphere-sealed condition. This yielded a film having a macroscopic self-assembly, as shown in Figures 4 and S10, confirming the applicability of our method. A closer look at the SEM image of the film revealed that the microparticles on the outer ring (Figure 4a) were smaller, with a mean average center-to-center distance of 115.6 ± 13.4 μm in length, in comparison to those inside the ring, which were bigger microparticle–microparticle distance 152.2 ± 13.9 μm in length (Figure 4b). This indicates that the retention time of the solvent governs the complete growth of microparticle size because the solvent evaporates faster from the edges than in the middle of a droplet of solution. We have also tested other molecules, such as 2-phenyl-*N*-methylfulleropyrrolidine and 4-tetradecyloxyazobenzene, which are representative compounds without alkyl chains on **1** and alkyl-π with smaller π units, respectively. However, the lack of appropriate hydrophobic amphiphilicity and balance between π-π interactions and van der Waals forces of alkyl chains did not produce such uniform macroscopic self-assembly (Figure S11).

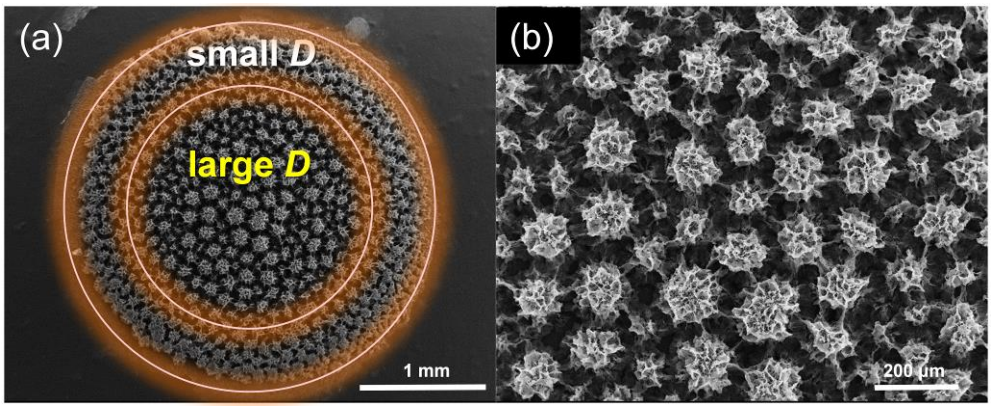

Figure 4. SEM images of a) $PC_{61}BM$ film formed by restricted evaporation of solvents (benzene: cumene) over three weeks at atmosphere-sealed air/water interface at 15 °C, showing smaller microparticle diameter at the outer surface and larger microparticle diameter inside; b) enlarged center area.

Based on the above interpretation, we discuss the mechanism of formation of the macroscopic self-assembly of these C_{60} derivatives (Figure 5). In the case of **1**, the benzene (or toluene) solution **1** initially homogeneously spreads over the air/water interface. The early stage of formation of macroscopic assembly, which finally results in hexagonal

array formation akin to the compound eye structure referred to as "Precursor domains," may form at the benzene/water interface. The plausible molecular configuration and alignment of **1** on a precursor domain leading to hexagonal packing of the micro-domes could occur due to the net-dipole repulsion in neighboring precursor domains (Figure 5a) [49-53]. The morphological distinction of Langmuir films was confirmed by SEM images of a Langmuir-Schaeffer transferred film (Figure 5b). A circular pattern was observed on the film surface, corresponding to the initial formation of domes. The formation of precursor domains at the benzene/water interface can be explained as follows. Due to slight hydrophobic differences in alkyl-C_{60} derivatives [37,42-48], the molecule acts as a pseudo-molecular dipole. The long-range repulsion between these domains composed of unidirectional molecular dipole [49-53] helps form a hexagonally-packed macroscopic assembly. To understand the assembly phenomena and molecular configuration of hydrophobic amphiphiles **1** on the precursor domains, *in-situ* Infrared Reflection Absorption Spectroscopy IRRAS (Figure 5c) and *in-situ* UV-Vis reflection spectroscopy (Figure 5d) were conducted. The alkyl chains were in crystalline-like states with *all-trans* rich conformation regardless of compression points, indicating solvophobic interaction between the alkyl chains as one of the driving interactions in the self-assembly process. The intermolecular interactions among **1** allow them to assemble a structure without additional forces. The structural assembly is likely self-driven as soon as **1** is introduced onto the water surface. In the case of C_{60} moiety, the two C_{60} absorption bands were not altered during the solvent evaporation (Figure 5d). Hence, during the casting, the intermolecular forces induce **1** to self-organize at the very early stage of the assembly process; the process cannot be captured with the techniques used here. To achieve a smooth film, surface tension should be uniform throughout the upper solution surface during the drying process. In the case of hexagonal-like packing in the convection of oil on water, solvent evaporation causes differences in temperature, surface tension, solvent concentration, and density within the solution. To compensate for the non-equilibrium conditions, a convection current starts at solution surfaces, forming macroscopically visible cell structures known as Bénard cells [54,55]. The difference in surface tension between the centers (lower) and edges (higher) of the solution results in the unevenness of the surface of the film after drying. However, in our case, convection of the upper solution during the solvent evaporation could be minimized due to controlled slow evaporation (2 days–3 weeks) under a constant cooled temperature (15 °C). It makes a hemispherical circle bottom shape instead of a honeycomb-like framework formation (Figures 5b and 5e). Here, solvent evaporation plays an important role in controlling the size of microparticles; evaporation is faster at the air/benzene interface than at the benzene/water interface. Thus, nano-aggregates could form at the air/benzene interface. The nano-aggregates were observed in HR-TEM (Figure 3b). An early sample was collected and examined to understand microparticles' growth. Figure 5e shows an SEM image of the half-grown film: the hemispherical shape was immature, with complete microparticles yet to be created. We have also performed FTIR and UV-Vis measurements of the immature particles, the samples from a later stage of precursor domain formation (Figure S12). These experimental results were consistent with our *in-situ* experiments, revealing that self-organization starts early. As seen in the immature hemispherical assembly formation, on the top of the precursor domain, nano-aggregates formed through supersaturation at the air/benzene interface pile up with an amorphous phase to create a hemispherical dome structure (Figure 5f). Simultaneously, the precursor domain can be grown until the solvent evaporation passes through its position in the self-assembly array film. This is also supported by our experiment shown in Figures S2 and S3, which revealed how benzene and toluene affect the size of microparticles. As benzene has a lower boiling point (80.1 °C) than toluene (110.6 °C), it evaporates faster, resulting in smaller microparticles. Further, the retention time also affects the sizes of domains and their distribution (Figure S7). Domains at the solvent/water interface have a longer retention time to form fully-grown microparticles. In contrast, those at the air/solvent interface (edges) do not due to the shorter retention time (Figure 4a).

In general, the kinetic spreading must be fast enough to overcome the aggregation process to ensure a uniform distribution. In this regard, benzene and CH_2Cl_2 exhibit excellent spreading properties for forming a uniform film. However, the growth of microparticle arrays requires slow evaporation of solvent; this minimizes the growth of microparticles at the air/solute interface. CH_2Cl_2 evaporates too fast for such array formation. On the other hand, *m*-xylene evaporates slower but fails to spread the molecules well. Out of all the solvents evaluated here, only benzene and toluene fulfill both criteria for fabricating unique anisotropic microparticle arrays of **1**. The importance of these factors was also confirmed by using 20% alcohol in water as a spreading medium. Such a substitute prevented structure formation even when benzene solution was used. The extent of disruption is correlated with the degree of change in the surface tension (Figure S4). We conclude that primarily, if not exclusively, the structural formation can be controlled by a delicate balance among various factors, including the type of solvent, concentration, surface tension for proper surface distribution, and precipitation rate. If the molecule has an excessive tendency to aggregate, ordered structures do not result. This was the case with pristine fullerene (C_{60}). We applied our method to $PC_{61}BM$, a fullerene derivative composed of C_{60} and alkyl chains moieties, which is similar to **1**; π-π and van der Waals forces, as well as weak hydrophobic amphiphilicity, resulted in an ordered structure from a mixed solvent of benzene and cumene with longer film growth time.

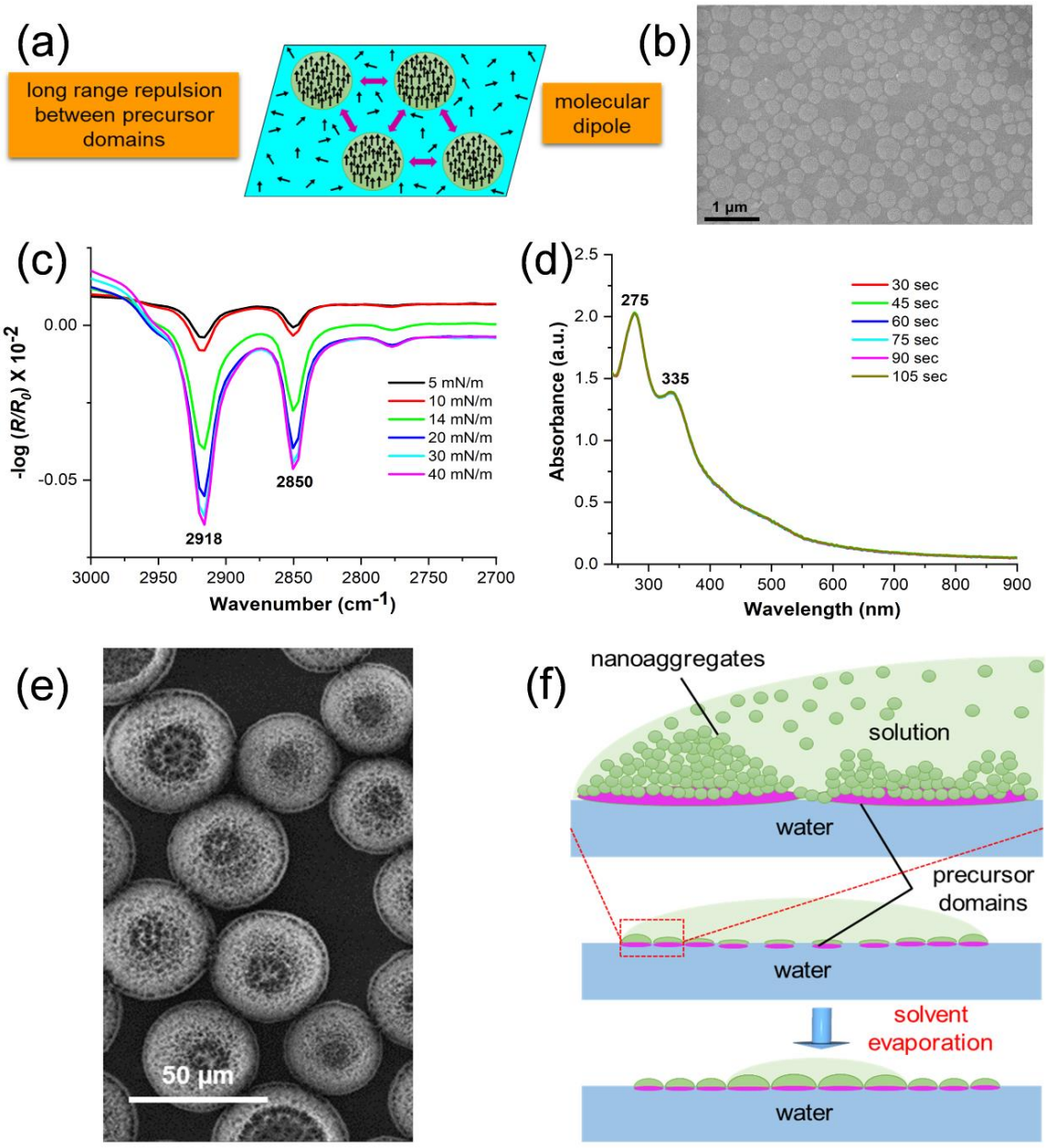

Figure 5. a) Schematic shows long-range repulsion between precursor domains happened at benzene/water interface [47]; b) SEM image for a film of **1** formed at Langmuir trough under open-air condition, obtained from early sample collection, transference by Langmuir-Schaeffer method; c) IRRAS at various compression stages, alkyl chains exhibit peaks at 2850 (υ_{sym}-CH_2) and 2918 cm^{-1} (υ_{asym}-CH_2); d) UV-Vis reflection spectra taken during the evaporation of benzene after the solution was spread onto the water surface; e) SEM image of immature hemispherical particles of **1**, obtained from early sample collection; and f) Schematic showing how nano-aggregates formed through supersaturation at the air/solution interface pile up together with amorphous phase on top of precursor microdomains at the solution/water interface.

4. Conclusion

This work provides a relatively simple and convenient route for forming kinetically controlled hierarchical molecular assemblies with stable, highly precise (approximately 38 µm microparticle-to-microparticle distance and long-range ordering up to 1.3 centimeters) from an alkyl-fullerene derivative. This could pave the way for achieving individual molecular assemblies up to multi-scale length in 3D structures by simply controlling solvent evaporation at the air/water interface under atmosphere-sealed conditions. The structural formation arises from a delicate balance among the solvent used and concentration. The method's feasibility was confirmed by forming a similar pattern of hexagonally-

packed larger microparticles (approximately 152 μm in size) from another fullerene derivative, $PC_{61}BM$, utilizing a similar protocol. Therefore, the present approach provides a facile fabrication method via a single procedure at non-equilibrium conditions, opening up a new paradigm in molecular self-assembly chemistry, patterning technology, and biomimetic science. Trials for preparing a surface-enhanced Raman analytical tool by transcribing the hexagonal array of hemispherical microparticles to Au metal film are currently undergoing in our laboratory.

Acknowledgments

We would like to pay our gratitude and respects to our former supervisor and friend, Prof. Helmuth Möhwald. He has tremendously contributed to this paper by providing critical and essential insights. This work would not have been possible without his advice and encouragement. T.N. acknowledges the financial support by Grants-in-Aid for Scientific Research (JSPS KAKENHI Grant Number JP18H03922, 24H01733 and 20F40041) and by World Premier International Research Center Initiative (WPI), MEXT, Japan. R.K.G. thanks for NIMS and JSPS Postdoctoral fellowship (P20041). J. J. G.-C. acknowledges the Spanish Ministry of Science and Innovation for the PID2020-112744GB-I00 project. We thank the Electron Microscopy Analysis Station of the National Institute for Materials Science for supporting FIB. We also express our thanks to Ms. M. Matsuda for her careful optimization of experimental conditions.

Data availability statement

The following files are available free of charge. Additional SEM images formed from various solvents, surface tension experiments and growth mechanism, SEM images and structure for applicability of the method, Langmuir trough film, film state UV-Vis, IR, XRD profile of $PC_{61}BM$, IRRAS and *in-situ* UV-Vis, SEM images of $PC_{61}BM$ film under various conditions, FTIR and UV-Vis of immature hemispherical particles (PDF)

Author Contributions

RKG and HA organized and wrote the manuscript, RKG and HA conducted experiments related to the macroscopic film formation, JJGC conducted the Langmuir trough experiment and *in-situ* IRRAS and UV-Vis spectroscopy, AH conducted the FIB-SIM analysis, TO conducted the HR-cryo-TEM analysis, and TN conceived the overall project, supervised and edited the manuscript. All authors have approved the final version of the manuscript.

‡R.K.G. and H.A. contributed equally.

Present Address:

[§]Department of Physical Chemistry, Faculty of Sciences, University of Cordoba, E-14071 Cordoba, Spain.

Declarations

The authors declare no competing financial interest.

References

[1] Whitesides G M and Grzybowski B 2002 Self-assembly at all scales *Science* **295** 2418–2421.

[2] Freeman R, Han M, Álvarez Z, Lewis J A, Wester J R, Stephanopoulos N, McClendon M T, Lynsky C, Godbe J M, Sangji H, Luijten E and Stupp S I 2018 Reversible self-assembly of superstructured networks *Science* **362** 808–813.

[3] Zhang S 2003 Fabrication of novel biomaterials through molecular self-assembly *Nat. Biotech.* **21** 1171–1178.

[4] Dong A, Chen J, Vora P M, Kikkawa J M and Murray C B 2010 Binary nanocrystal superlattice membranes self-assembled at the liquid–air interface *Nature* **466** 474–477.

[5] Lai W-H, Wang Y-X, Wang Y, Wu M, Wang J-Z, Liu H-K, Chou S-L, Chen J and Dou S-X 2019 Morphology tuning of inorganic nanomaterials grown by precipitation through control of electrolytic dissociation and supersaturation *Nat. Chem.* **11** 695–701.

[6] Grill L, Dyer M, Lafferentz L, Persson M, Peters M V and Hecht S 2007 Nano-architectures by covalent assembly of molecular building blocks *Nat. Nanotech.* **2** 687–691.

[7] Chen X, Geng K, Liu R, Tan K T, Gong Y, Li Z, Tao S, Jiang Q and Jiang D 2020 Covalent organic frameworks: chemical approaches to designer structures and built-in functions *Angew. Chem. Int. Ed.* **59** 5050–5091.

[8] Li Y, Guo L, Lv Y, Zhao Z, Ma Y, Chen W, Xing G, Jiang D and Chen L 2021 Polymorphism of 2D imine covalent organic frameworks *Angew. Chem. Int. Ed.* **60** 5363–5369.

[9] Tan F, Han S, Peng D, Wang H, Yang J, Zhao P, Ye X, Dong X, Zheng Y, Zheng N, Gong L, Liang C, Frese N, Gölzhäuser A, Qi H, Chen S, Liu W and Zheng Z 2021 Nanoporous and highly thermal conductive thin film of single-crystal covalent organic frameworks ribbons *J. Am. Chem. Soc.* **143** 3927–3933.

[10] Sakamoto R, Hoshiko K, Liu Q, Yagi T, Nagayama T, Kusaka S, Tsuchiya M, Kitagawa Y, Wong W-Y and Nishihara H 2015 A photofunctional bottom-up bis (dipyrrinato) zinc (II) complex nanosheet *Nat. Commun.* **6** 6713.

[11] Matsumoto M, Valentino L, Stiehl G M, Balch H B, Corcos A R, Wang F, Ralph D C Mariñas B J and Dichtel W R 2018 Lewis-acid-catalyzed interfacial polymerization of covalent organic framework films *Chem* **4** 308–317.

[12] Sahabudeen H, Qi H, Ballabio M, Položij M, Olthof S, Shivhare R, Jing Y, Park S, Liu K, Zhang T, Ma J,

Rellinghaus B, Mannsfeld S, Heine T, Bonn M, Cánovas E, Zheng Z, Kaiser U, Dong R and Feng X 2020 Highly crystalline and semiconducting imine-based two-dimensional polymers enabled by interfacial synthesis *Angew. Chem. Int. Ed.* **59** 6028–6036.

[13] Liu K, Qi H, Dong R, Shivhare R, Addicoat M, Zhang T, Sahabudeen H, Heine T, Mannsfeld S, Kaiser U, Zheng Z and Feng X 2019 On-water surface synthesis of crystalline, few-layer two-dimensional polymers assisted by surfactant monolayers *Nat. Chem.* **11** 994–1000.

[14] Park S, Liao Z, Ibarlucea B, Qi H, Lin H H, Becker D, Melidonie J, Zhang T, Sahabudeen H, Baraban L, Baek C, Zheng Z, Zschech E, Fery A, Heine T, Kaiser U, Cuniberti G, Dong R and Feng X 2020 Two-dimensional boronate ester covalent organic framework thin films with large single crystalline domains for a neuromorphic memory device *Angew. Chem. Int. Ed.* **132** 8295–8301.

[15] Schneemann A, Dong R, Schwotzer F, Zhong H, Senkovska I, Feng X and Kaskel S 2021 2D framework materials for energy applications *Chem. Sci.* **12** 1600–1619.

[16] Li C, Cho J, Yamada K, Hashizume D, Araoka F, Takezoe H, Aida T and Ishida Y 2015 Macroscopic ordering of helical pores for arraying guest molecules noncentrosymmetrically *Nat. Commun.* **6** 8811.

[17] Widawski G, Rawiso M and François B 1994 Self-organized honeycomb morphology of star-polymer polystyrene films *Nature* **369** 387–389.

[18] Song L, Bly R K, Wilson J N, Bakbak S, Park J O, Srinivasarao M and Bunz U H F 2004 Facile Microstructuring of Organic Semiconducting Polymers by the Breath Figure Method: Hexagonally Ordered Bubble Arrays in Rigid Rod-Polymers *Adv. Mater.* **16** 115–118.

[19] Lafferentz L, Eberhardt V, Dri C, Africh C, Comelli G, Esch F, Hecht S and Grill L 2012 Controlling on-surface polymerization by hierarchical and substrate-directed growth *Nat. Chem.* **4** 215–220.

[20] Kissel P, Murray D J, Wulftange W J, Catalano V J and King B T 2014 A nanoporous two-dimensional polymer by single-crystal-to-single-crystal photopolymerization *Nat. Chem.* **6** 774–778.

[21] Colson J W and Dichtel W R 2013 Rationally synthesized two-dimensional polymers *Nat. Chem.* **5** 453–465.

[22] Kissel P, Erni R, Schweizer W, Rossell M, King B, Bauer T, Götzinger S, Schlüter A and Sakamoto J 2012 A two-dimensional polymer prepared by organic synthesis *Nat. Chem.* **4** 287–291.

[23] Galeotti G, De Marchi F, Hamzehpoor E, MacLean O, Rao M R, Chen Y, Besteiro L V, Dettmann D, Ferrari L, Frezza F, Sheverdyaeva P M, Liu R, Kundu A K, Moras P, Ebrahimi M, Gallagher M C, Rosei F, Perepichka D F and Contini G 2020 Synthesis of mesoscale ordered two-dimensional π-conjugated polymers with semiconducting properties *Nat. Mater.* **19** 874–880.

[24] Zhang X and Takeuchi M 2009 Controlled Fabrication of Fullerene C_{60} into Microspheres of Nanoplates through Porphyrin-Polymer-Assisted Self-Assembly *Angew. Chem. Int. Ed.* **48** 9646–9651.

[25] Yabu H and Shimomura M 2005 Simple fabrication of microlens arrays *Langmuir* **21** 1709–1711.

[26] Karthaus O, Maruyama N, Cieren X, Shimomura M, Hasegawa H and Hashimoto T 2000 Water-Assisted Formation of Micrometer-Size Honeycomb Patterns of Polymers *Langmuir* **16** 6071–6076.

[27] Sun Y, Lei Y, Hu W and Wong W-Y 2020 Epitaxial Growth of Nanorod Meshes from Luminescent Organic Cocrystals via Crystal Transformation *J. Am. Chem. Soc.* **142** 7265–7269.

[28] Kim J Y, Barcus K and Cohen S M 2021 Controlled Two-Dimensional Alignment of Metal–Organic Frameworks in Polymer Films *J. Am. Chem. Soc.* **143** 3703–3706.

[29] Kojima M, Hirai Y, Yabu H and Shimomura M 2009 The Effects of Interfacial Tensions of Amphiphilic Copolymers on Honeycomb-Patterned Films *Polym. J.* **41** 667–671.

[30] Sun Y, Chen C, Wang X, Zhang F, Lu S, Li X, Suo X and Lin Z 2020 Self-Assembly of Metallacages into Centimeter Films with Tunable Size and Emissions *J. Am. Chem. Soc.* **142** 17933–17937.

[31] Seiki N, Shoji Y, Kajitani T, Ishiwari F, Kosaka A, Hikima T, Takata M, Someya T and Fukushima T 2015 Rational synthesis of organic thin films with exceptional long-range structural integrity *Science* **348** 1122–1126.

[32] Dong A, Chen J, Vora P M, Kikkawa J M and Murray C B 2010 Binary nanocrystal superlattice membranes self-assembled at the liquid–air interface *Nature* **466** 474–477.

[33] Udayabhaskararao T, Altantzis T, Houben L, Coronado-Puchau M, Langer J, Popovitz-Biro R, Liz-Marzán L M, Vuković L, Král P, Bals S and Klajn R 2017 Tunable porous nanoallotropes prepared by post-assembly etching of binary nanoparticle superlattices *Science* **358** 514–518.

[34] Nakanishi T, Miyashita N, Michinobu T, Wakayama Y, Tsuruoka T, Ariga K and Kurth D G 2006 Perfectly straight nanowires of fullerenes bearing long alkyl chains on graphite *J. Am. Chem. Soc.* **128** 6328–6329.

[35] Gupta R K, Yoshida M, Saeki A, Guo Z and Nakanishi T 2023 Alkyl–C_{60} liquid electrets as deformable mechanoelectric generators *Mater. Horiz.* **10** 3458–3466.

[36] Nakanishi T, Michinobu T, Yoshida K, Shirahata N, Ariga K, Möhwald H and Kurth D G 2008 Nanocarbon Superhydrophobic Surfaces created from Fullerene-Based Hierarchical Supramolecular Assemblies *Adv. Mater.* **20** 443–446.

[37] Asanuma H, Li H, Nakanishi T and Möhwald H 2010 Fullerene derivatives that bear aliphatic chains as

unusual surfactants: hierarchical self-organization, diverse morphologies, and functions *Chem. Eur. J.* ***16*** 9330–9338.

[38] Nakanishi T 2010 Supramolecular soft and hard materials based on self-assembly algorithms of alkyl-conjugated fullerenes *Chem. Commun.* **46** 3425–3436.

[39] Kim S H, Misner M J, Xu T, Kimura M and Russell T P 2004 Highly oriented and ordered arrays from block copolymers via solvent evaporation *Adv. Mater.* **16** 226–231.

[40] Vazquez G, Alvarez E and Navaza J M 1995 Surface tension of alcohol water + water from 20 to 50. degree C. *J. Chem. Eng. Data* **40** 611–614.

[41] Snyder R G 1967 Vibrational study of the chain conformation of the liquid n-paraffins and molten polyethylene *J. Chem. Phys.* **47** 1316–1360.

[42] Hollamby M J, Karny M, Bomans P H, Sommerdjik N A, Saeki A, Seki S, Minamikawa H, Grillo I, Pauw B R, Brown P, Eastoe J, Möhwald H and Nakanishi T 2014 Directed assembly of optoelectronically active alkyl–π-conjugated molecules by adding n-alkanes or π-conjugated species *Nat. Chem.* **6** 690–696.

[43] Mouri E, Nakanishi T, Nakashima N and Matsuoka H 2002 Nanostructure of fullerene-bearing artificial lipid monolayer on water surface by in situ X-ray reflectometry *Langmuir* **18** 10042–10045.

[44] Yang L, Shirahata N, Saini G, Zhang F, Pei L, Asplund M C, Kurth D G, Ariga K, Sautter K. Nakanishi T, Smentkowski V and Linford M R 2009 Effect of surface free energy on PDMS transfer in microcontact printing and its application to ToF-SIMS to probe surface energies *Langmuir* **25** 5674–5683.

[45] Lu F, Neal E A and Nakanishi T 2019 Self-assembled and nonassembled alkylated-fullerene materials *Acc. Chem. Res.* **52** 1834–1843.

[46] Neal E A and Nakanishi T 2021 Alkyl-Fullerene materials of tunable morphology and function *Bull. Chem. Soc. Jpn.* **94** 1769–1788.

[47] Zheng X, Gupta R K and Nakanishi T 2022 Order from disorder: directed assembly of alkyl-π functional molecular liquids *Curr. Opin. Colloid Interface Sci.* **62** 101641.

[48] Tateyama A and Nakanishi T 2023 Responsive molecular liquid materials *Responsive Mater.* **1** e20230001.

[49] Möhwald H 1990 Phospholipid and phospholipid-protein monolayers at the air/water interface *Annu. Rev. Phys. Chem.* **41** 441–476.

[50] Giner-Casares J J, Brezesinski G and Möhwald H 2014 Langmuir monolayers as unique physical models *Curr. Opin. Colloid Interface Sci.* **19** 176–182.

[51] Wu C, Bergman D, Balents L and Das Sarma S 2007 Flat bands and Wigner crystallization in the honeycomb optical lattice *Phys. Rev. Lett.* **99** 070401.

[52] Boudjada N, Buessen F L and Paramekanti A 2021 Molecular dipoles in designer honeycomb lattices *Phys. Rev. B* **103** 165408.

[53] Smoleński T, Dolgirev P E, Kuhlenkamp C, Popert A, Shimazaki Y, Back P, Lu X, Kroner M, Watanabe K, Taniguchi T, Esterlis I, Demler E and Imamoğlu A 2021 Signatures of Wigner crystal of electrons in a monolayer semiconductor *Nature* **595** 53–57.

[54] Bénard H 1901 The cellular whirlpools in a liquid sheet transporting heat by convection in a permanent regime *Ann. Chim. Phys.* **23** 62–144.

[55] Koschmieder E L 1993 Bénard Cells and Taylor Vortices *Cambridge University Press, Cambridge*.